

## Phase Signature of Topological Transition in Josephson Junctions

Matthieu C. Dartiailh<sup>1</sup>, William Mayer<sup>1</sup>, Joseph Yuan<sup>1</sup>, Kaushini S. Wickramasinghe<sup>1</sup>, Alex Matos-Abiague<sup>2</sup>, Igor Žutić<sup>3</sup>, and Javad Shabani<sup>1</sup>

<sup>1</sup>Center for Quantum Phenomena, Department of Physics, New York University, New York, New York 10003, USA

<sup>2</sup>Department of Physics and Astronomy, Wayne State University, Detroit, Michigan 48201, USA

<sup>3</sup>Department of Physics, University at Buffalo, State University of New York, Buffalo, New York 14260, USA



(Received 18 June 2020; accepted 16 December 2020; published 21 January 2021)

Topological superconductivity holds promise for fault-tolerant quantum computing. While planar Josephson junctions are attractive candidates to realize this exotic state, direct phase measurements as the fingerprint of the topological transition are missing. By embedding two gate-tunable Al/InAs Josephson junctions in a loop geometry, we measure a  $\pi$  jump in the junction phase with an increasing in-plane magnetic field  $B_{\parallel}$ . This jump is accompanied by a minimum of the critical current, indicating a closing and reopening of the superconducting gap, strongly anisotropic in  $B_{\parallel}$ . Our theory confirms that these signatures of a topological transition are compatible with the emergence of Majorana bound states.

DOI: 10.1103/PhysRevLett.126.036802

Majorana bound states (MBS), which are their own antiparticles, are predicted to emerge as zero-energy modes localized at the boundary between a topological superconductor and a topologically trivial region [1]. MBS can nonlocally store quantum information, and their non-Abelian exchange statistics allow for the implementation of quantum gates through braiding operations [2]. This makes them ideal candidates for robust qubits in fault-tolerant topological quantum computing [3]. Rather than seeking elusive spinless p-wave superconductors required for MBS, a common approach is to use conventional s-wave superconductors to proximity-modify semiconductor heterostructures with suitable symmetries [4].

Early MBS proposals were focused on one-dimensional (1D) systems such as proximitized nanowires and atomic chains [5–9], where the observation of a quantized zero-bias conductance peak (ZBCP) [10] provided the support for MBS. However, the inherent difficulties in the technological implementation of the required networks and the intrinsic instabilities of their 1D elements have motivated the search for versatile 2D platforms using more conventional devices such as Josephson junctions (JJs) and spin valves [11–18]. Recent experiments [13,14] suggest that planar JJs are particularly promising because they support topological superconductivity over a large parameter range. The change between trivial and topological superconductivity, probed by ZBCP, is realized by applying an in-plane magnetic field,  $B_{\parallel}$ , and biasing the superconducting phase between 0 and  $\pi$ . This is achieved by embedding the JJ in a loop [13] or by using two strongly asymmetric JJs [14] in a superconducting quantum interference device (SQUID).

Since ZBCP could arise even without topological superconductivity, it is crucial to identify alternative signatures. A striking example is the closing and reopening of the

superconducting gap with an increasing  $B_{\parallel}$  that is simultaneously accompanied by a phase jump [4–6,19–21]. Direct phase measurements have proven to be a powerful probe to elucidate unconventional superconductivity [22]. A trivial Zeeman exchange  $0-\pi$  transition can happen without spin-orbit coupling (SOC) [23,24] but is then expected to be independent of the  $B_{\parallel}$  direction in contrast to the case of topological superconductivity. It was also proposed that a Zeeman-driven Fulde-Ferrell-Larkin-Ovchinnikov (FFLO)-like mechanism could lead to a minimum in the critical current,  $I_c$ , through a spatial variation of the superconducting order parameter [18]. This mechanism can be characterized by the required to reach the first minimum,

$$B_{\text{FFLO}} = \frac{\pi \hbar v_F}{2 g \mu_B L}, \quad (1)$$

where  $\hbar$  is the Dirac constant,  $v_F$  the Fermi velocity,  $g$  the effective  $g$  factor,  $\mu_B$  the Bohr magneton, and  $L$  the distance between the superconducting contacts.

In Fig. 1(a), we plot  $B_{\text{FFLO}}$  as a function of the distance between the contacts for JJs on HgTe [18], InSb [17], and Bi nanowires [25], and InAs for a range of  $v_F$  noted in the caption. This expression is in a good agreement with the published measurements (see also Sec. III of the Supplemental Material [26]). In this Letter, we consider a device fabricated on an InAs quantum well with a  $g$  factor of 10 and effective mass of  $m^* \approx 0.03$  electron mass [11]. For  $L = 100$  nm, using  $|g| = 10$  and  $n = 7 \times 10^{11}$  cm<sup>-2</sup>,  $v_F = \hbar \sqrt{2\pi n}/m^* \approx 8 \times 10^5$  m/s, we find from Eq. (1) an estimate for the trivial  $0-\pi$  transition at  $B_{\text{FFLO}} \approx 14.4$  T, still much higher than any  $B_{\parallel}$  used in our study.

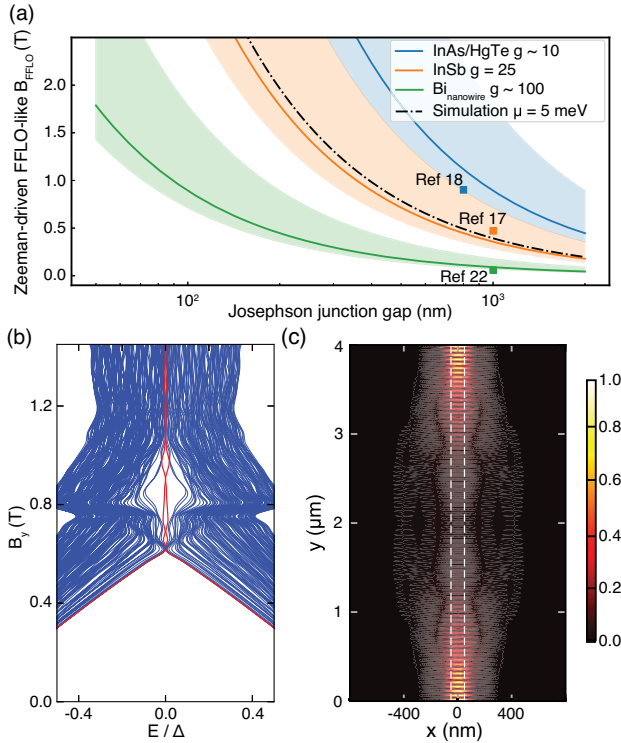


FIG. 1. Signatures of trivial and topological superconductivity. (a) Predicted field at which a Zeeman-driven FFLO-like mechanism [18] leads to a minimum in  $I_c$  as a function of the separation between the superconducting contacts. Solid line:  $v_F = 5 \times 10^5$  m/s. Colored region: from  $4 \times 10^5$  m/s to  $1 \times 10^6$  m/s. Dashed line: our simulation for which the FFLO-like mechanism would induce a transition at  $\approx 4$  T. (b) The low-energy ground-state spectrum of a JJ with a superconducting region at  $\mu = 5.05$  meV. The energy gap closes and reopens, indicating a topological phase transition and the emergence of an MBS. Red lines: the evolution of finite-energy states into MBS inside the topological gap  $\lesssim 23$   $\mu\text{eV}$ . (c) Probability density of MBS in the JJ for  $B = 0.85$  T, normalized to its maximum value. It clearly indicates the formation of the MBS localized at the end of the junction. White lines: the edges of the normal region.

With  $B_{\parallel}$  along the  $y$  direction, tight-binding simulations presented in Figs. 1(b) and 1(c) predict a single junction, without a phase bias, will undergo a topological phase transition at  $B_y > 0$ . A hallmark of this transition is the closing and reopening of the superconducting gap [4,19–21] manifested as a minimum in  $I_c$  shown in Figs. S8(a) and S8(d) of [26]. Above that closing, the system is in a topological phase dominated by chiral p-type superconductivity and host MBS localized at each end of the JJ as shown in Fig. 1(c). This is in contrast to a phase-biased junction [13,14], which, at  $\pi$  phase, can exhibit a topological phase at an arbitrarily low  $B_y$ .

Unlike the prior works [13,14], in our JJs the phase is not biased. Instead, it self-adjusts to minimize the free energy of the system in both the trivial and topological phases. We demonstrate how two gate-tunable and nearly symmetric

JJs forming a SQUID provide a platform to realize the first direct phase-sensitive measurements of a topological transition. This is a complementary evidence for the topological nature of our observation of a minimum in  $I_c$ .

The JJs based on epitaxial Al/InAs [11] are engineered to support high-interfacial transparency and high mobility resulting in JJ transparency  $\tau \approx 0.9$ , as estimated from the current-phase relation [27], and robust proximity-induced superconductivity in InAs. Both junctions (1, 2) of the SQUID are  $W = 4$   $\mu\text{m}$  wide and  $L = 100$  nm long, while the area of the SQUID loop is  $25$   $\mu\text{m}^2$ . The superconducting gap of the aluminium layer  $\Delta_0 = 230 \pm 10$   $\mu\text{eV}$  is estimated from measured critical temperature. With the coherence length  $\xi_0 = \hbar v_F / (\pi \Delta_0) \approx 770$  nm and the mean free path,  $l_e \approx 200$  nm [27], the JJs are in a quasiballistic short-junction limit,  $l_e > L$  and  $\xi_0 \gg L$  [26,28]. At high density ( $n \approx 2 \times 10^{12}$   $\text{cm}^{-2}$ ), based on previous study [29], we expect the Rashba SOC strength to reach  $\alpha \approx 150$   $\text{meV \AA}$ , which corresponds to the spin-orbit energy  $E_{\text{SO}} = am^*v_F/\hbar \approx 5.3$  meV. We apply  $B_{\parallel}$  along an arbitrary axis defined by angle  $\theta$ . At  $\theta = 0$ , the field is along  $y$  and perpendicular to the current flowing through the JJ. We can also impose a phase difference between the two JJs by applying a small out-of-plane field. The versatility of our setup comes from the possibility of operating it either as a SQUID or as a single JJ by fully depleting the other JJ.

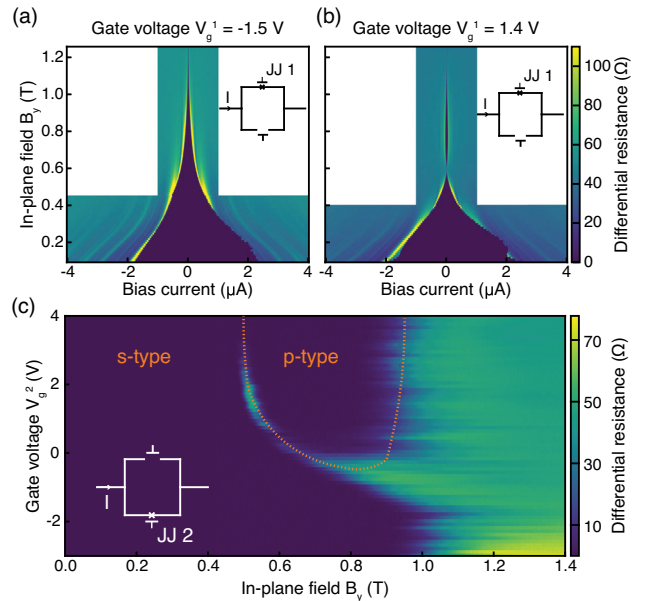


FIG. 2. Gate control of trivial and topological superconductivity. Measurement of the differential resistance of JJ1 as function of an applied in-plane field along the  $y$  axis at two different gate voltages: (a)  $V_g^1 = -1.5$  V, (b)  $V_g^1 = 1.4$  V. In both cases, JJ2 is depleted ( $V_g^2 = -7$  V) and does not participate in the transport. At high gate (b), a minimum of the critical current is observed around 600 mT for JJ1. (c) Zero-bias differential resistance of JJ2 as a function of the applied in-plane field and the gate voltage.  $V_g^1$  is set to  $-7$  V.

We next consider the  $B_y$  dependence of the JJ1 critical current. In Fig. 2(a), at lower  $V_g^1 = -1.5$  V and thus at a lower density, we observe a trivial monotonic decrease of  $I_c$  with  $B_y$ . Remarkably, at higher  $V_g^1 = 1.4$  V in Fig. 2(b), we see a striking difference with a nonmonotonic behavior of  $I_c$  and a minimum around  $B_y = 600$  mT in agreement with the tight-binding results from Fig. S8(d) [26]. Above that minimum, we measure  $I_c \approx 20$  nA, consistent with the gap reopening and topological transition. After the minimum, the resistance vanishes for  $I < I_c$ . In contrast, after gap closing, only nonzero resistance was measured in Ref. [18].

Minima in  $I_c$  have been observed in Ref. [14] due to orbital effects, which can become energetically unfavorable in the presence of a strong proximity effect [30]. We expect that the proximity effect is stronger in our samples since the top barrier of our 2D electron gas is more transparent due to the lower band gap and electron mass of (In,Ga)As at 81% In content compared to the 75% In content used in [14]. We discuss this point in greater detail in [26].

Previous works [19,20] have focused on the low-density and long-junction limit. In those works, the topological transition was found to happen at the Zeeman energy  $E_Z = g\mu_B B_{||}/2 \approx E_T/2$ , where the Thouless energy is  $E_T = (\pi/2)\hbar v_F/L$  [20]. While this relation is equivalent to Eq. (1), the Thouless energy in the ballistic regime is not uniquely defined [17,40]. These models do not apply to the short and high- $n$  junctions studied in this work for which  $E_T \propto \sqrt{n}/L$  becomes larger ( $\approx 8.4$  meV). The inadequacy of those models has also been pointed out in Ref. [14], which has motivated subsequent studies [30], as well as in our own simulations [26], confirming that the topological transition observed in our system is no longer determined by  $E_Z = E_T/2$ . However, we find that as  $L$  increases, the transition field approaches the value predicted by Eq. (1) [26]. This is consistent with the derivation of Eq. (1), where the effective  $g$  factor was assumed to be finite only in the normal region. In our system, we consider a finite  $g$  factor over the whole junction. Therefore, the agreement with  $E_Z = E_T/2$  is better when the normal region is long and the effects of finite  $g$  factor in the proximitized InAs layer become less relevant.

In our device, both JJs show a nontrivial evolution of the superconducting gap and topological transition. Figure 2(c) shows the zero-bias differential resistance of JJ2 as a function  $V_g^2$  and  $B_y$ . At the largest  $V_g^2$ , the transition occurs at  $\approx 500$  mT and moves toward higher  $B_y$  as  $V_g^2$  is decreased. Below  $V_g^2 = -1.5$  V, no evidence of any transition remains. The lower  $B_y$  transition in JJ2 compared to JJ1 can be attributed to small variation of junction properties, for example, lower supercurrent and the corresponding induced gap.

While the observed nonmonotonic dependence of  $I_c$  with  $B_y$  is consistent with a transition to topological superconductivity, phase-sensitive measurements with a SQUID could independently confirm this scenario. However, it is

generally difficult to avoid arbitrary field offsets between measurements. Here, following the approach described in Ref. [27], we use the gate tunability of our device to measure the phase offset between the oscillations observed at a different gate voltage. We avoid the issue of the field offset by performing a single  $B_z$  sweep and measuring  $I_c$  at a different gate voltage value for each value of the externally applied field. This procedure is valid, since changing the asymmetry between the  $I_c$  of the two JJs does not affect the position of the maximum of the critical current in the SQUID [27].

Using SQUID interferometry, we can identify a topological transition by setting JJ1 at  $V_g^1 = -2$  V as the reference junction. At this  $V_g^1$ , JJ1 does not show a topological transition at any  $B_y$ . The resulting SQUID oscillations in JJ2 reveal crucial differences between  $B_y = 100$  mT and 850 mT, shown respectively in Figs. 3(a) and 3(b), for various  $V_g^2$ . From Fig. 2(c), we expect that JJ2 would never reach the topological regime at 100 mT. Indeed, in Fig. 3(a), we only observe a small phase shift, which we attribute to the interplay between the  $E_Z$  and SOC [23]. At a higher  $B_y$ , in Fig. 3(b), there is a larger phase shift between  $V_g^2 = -3$  V and  $-4$  V than in Fig. 3(a), consistent with the expected linear increase in  $B_y$  [23]. However, comparing  $V_g^2 = -1$  V and higher-gate values, a phase shift of about  $\pi$  occurs.

Our tight-binding calculations, presented in Figs. S8(a) and S8(d) [26], reveal that a phase jump is a signature expected for the topological transition with the emergence of MBS. As shown, the ground-state phase (minimizing the energy in the absence of current) exhibits a phase jump when the topological transition occurs. Because of the broadening in the phase jump, the phase changes from 0 to a value close to  $\pi$ , not at a precise value of the magnetic field but over a finite range of  $B_y$  [see Figs. S8(a) and S8(d)]. The phase jump broadening may cause a shift between the magnetic field at which the system transits into the topological state and the field at which the minimum of  $I_c$  occurs. Consequently, the topological transition occurs at a field smaller than or equal to the field corresponding to the  $I_c$  minimum. The broadening of the phase jump observed in the experiment appears to be smaller than the one in the numerical simulations, suggesting the phase transition and the measured  $I_c$  minimum occur at nearly the same  $B_y$ . In Fig. 3(c), we present the phase shift between the reference scan performed at  $V_g^2 = -4$  V and subsequent gate values. At low  $B_y$ , below the topological transition, we observe that the phase is linear in  $B_y$ , as indicated by the solid lines corresponding to linear fits to the values below 450 mT. The increase in slope with  $V_g^2$  can be attributed to the increase of SOC [27]. For  $V_g^2 = -3$  V and  $-1$  V, the linear trend holds over all  $B_y$ . However, for  $V_g^2 = 1$  V, 2 V, and 3 V, a jump can be observed around 550 mT, followed by another linear portion. To separate these effects, we subtract the linear component extracted from low- $B_y$  fits. The corrected phase

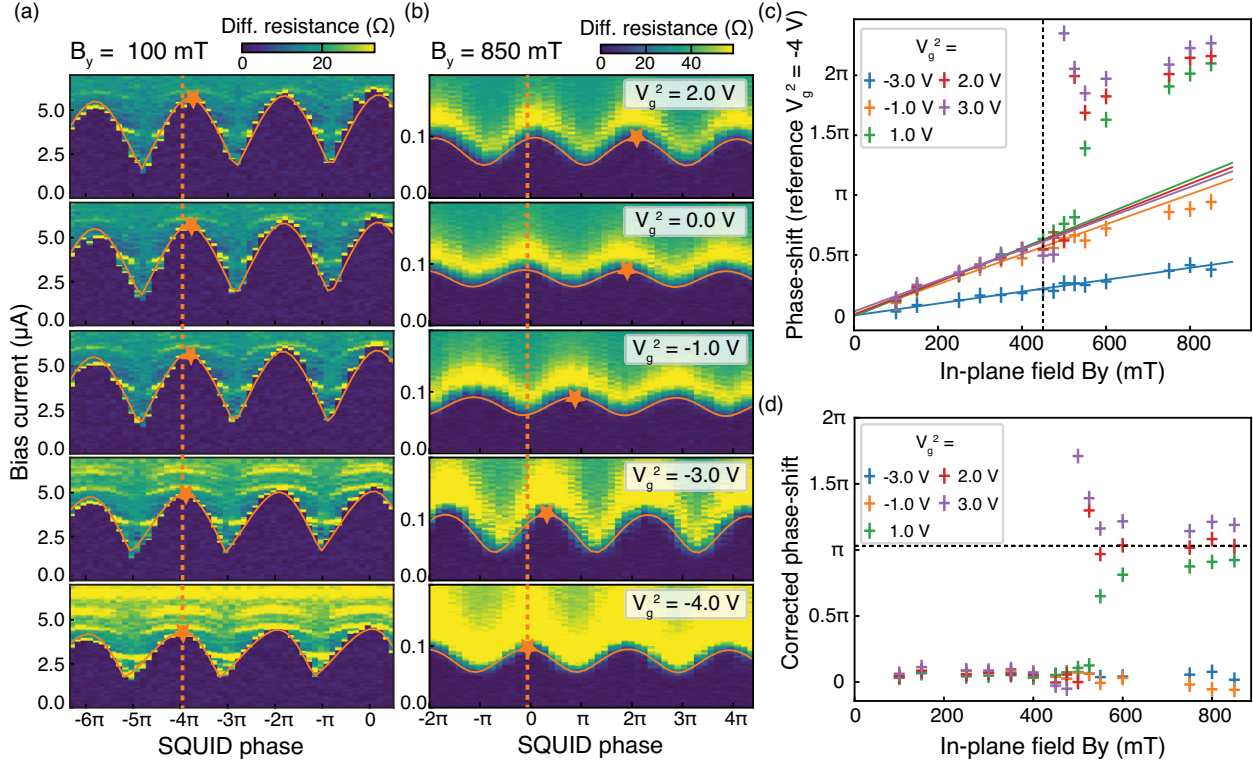


FIG. 3. Phase signature of topological transition from SQUID interferometry. SQUID oscillations for  $B_y = 100$  mT (a) and 850 mT (b) for different  $V_g^2$  at  $V_g^1 = -2$  V. Dashed lines: position of the maximum at  $V_g^2 = -4$  V used as a phase reference. Stars: position of the maximum of the oscillation. Solid lines: best fits to the SQUID oscillations used to extract the period and the phase shift between different  $V_g^2$ . (c) Phase difference between the SQUID oscillation at  $V_g^2 = -4$  V and the oscillation at a different value as a function of  $B_y$ . Solid lines: linear fits of the data for  $B_y \leq 450$  mT. (d) Phase shift from which the linear  $B_y$  contribution has been subtracted to highlight the phase jump of about  $\pi$  occurring for the three higher  $V_g^2$  values.

in Fig. 3(d) reveals a phase jump with a magnitude near  $\pi$ , which is around the  $I_c$  minimum. This is a strong evidence for the existence of a topological phase transition consistent with theoretical calculations presented in [26]. The observed phase jump rules out orbital effects that could lead to a minimum in the  $I_c$ , as predicted in Ref. [20]. For a JJ with symmetric contact geometry, in this case identical, such effects would not lead to a phase jump, and only the  $I_c$  minimum would be observed.

A distinct feature of the observed topological transition is its interplay of SOC and  $\mathbf{B}_{\parallel}$ . In our system, the topological regime is expected when  $\mathbf{B}_{\parallel}$  is along the  $y$  direction, i.e.,  $\theta = 0$ . Deviations from the  $y$  direction result in a decrease of the topological gap for  $\phi \lesssim \pi$  [31]. Therefore, for large enough  $\theta$ , no topological transition or associated minimum in  $I_c$  is expected. We test this by probing the  $I_c$  minimum in a tilted  $\mathbf{B}_{\parallel}$ , away from  $B_y$ . In Fig. 4, we show  $I_c$  enlargements of the JJ1 at  $V_g^1 = 1.4$  V. As  $\theta$  is increased, the  $I_c$  minimum increases but always occurs at the same value of  $B_y$ . If only the magnitude of  $E_Z$  was relevant, one would expect to see the minima move to lower values of  $B_y$ . Similarly, SQUID data at  $\theta = 10^\circ$  [26], display a reduced phase shift, which may indicate a reduced topological gap. In contrast to smaller angles, at  $\theta = 20^\circ$ ,  $I_c$

decreases monotonically, which suggests that s-wave order prevails and no transition is observed. This observation agrees with our calculations [26]. Unlike the insensitivity of

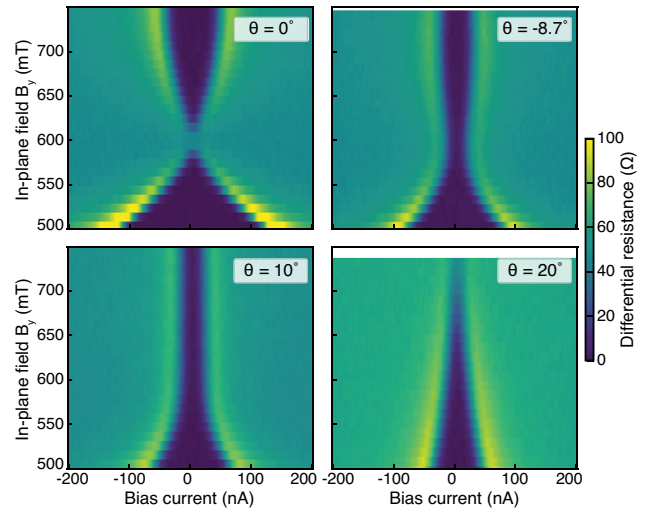


FIG. 4. In-plane magnetic-field anisotropy of the gap closing. Differential resistance of JJ1 as function of the bias current and the  $y$  component of  $\mathbf{B}_{\parallel}$ , applied at an angle  $\theta$  with respect to the  $y$  direction as depicted in Fig. 1(a).

trivial Zeeman  $0-\pi$  transitions to the in-plane field rotation, our strong dependence on the  $B_{\parallel}$  direction is further evidence for a topological  $0-\pi$  transition. Furthermore, while for 2D InAs quantum wells only an out-of-plane anisotropy of the  $g$  factor was measured [41], we found that even the presence of a small in-plane  $g$ -factor anisotropy could not alone explain our results in Fig. 4.

By embedding Al/InAs Josephson junctions in a nearly symmetric SQUID loop, we measured two distinct signatures of a topological phase transition, a minimum in  $I_c$  and the coincidental  $\pi$  jump of the superconducting phase, both indicative of a closing and reopening of the superconducting gap. Our findings demonstrate the emergence of a topological phase. In addition to  $B_y$ , the top gate voltage is shown to be an efficient control knob for manipulating the topological phase transition. This offers a scalable platform for detection and manipulation of Majorana bound states [42] and for development of complex circuits capable of fault-tolerant topological quantum computing. The versatility of this two-dimensional geometry and SQUID sensing may also advance studies of MBS using magnetic textures for topological superconductivity [43,44] and support other exotic states that can be probed by phase-sensitive signatures [45].

This work is supported by DARPA Topological Excitations in Electronics (TEE) program under Grant No. DP18AP900007.

- 
- [1] A. Y. Kitaev, Unpaired Majorana fermions in quantum wires, *Phys. Usp.* **44**, 131 (2001).
- [2] C. Nayak, S. H. Simon, A. Stern, M. Freedman, and S. Das Sarma, Non-Abelian anyons and topological quantum computation, *Rev. Mod. Phys.* **80**, 1083 (2008).
- [3] D. Aasen, M. Hell, R. V. Mishmash, A. Higginbotham, J. Danon, M. Leijnse, T. S. Jespersen, J. A. Folk, C. M. Marcus, K. Flensberg, and J. Alicea, Milestones Toward Majorana-Based Quantum Computing, *Phys. Rev. X* **6**, 031016 (2016).
- [4] L. Fu and C. L. Kane, Superconducting Proximity Effect and Majorana Fermions at the Surface of a Topological Insulator, *Phys. Rev. Lett.* **100**, 096407 (2008).
- [5] R. M. Lutchyn, J. D. Sau, and S. Das Sarma, Majorana Fermions and a Topological Phase Transition in Semiconductor-Superconductor Heterostructures, *Phys. Rev. Lett.* **105**, 077001 (2010).
- [6] Y. Oreg, G. Refael, and F. von Oppen, Helical Liquids and Majorana Bound States in Quantum Wires, *Phys. Rev. Lett.* **105**, 177002 (2010).
- [7] V. Mourik, K. Zuo, S. M. Frolov, S. R. Plissard, E. P. a. M. Bakkers, and L. P. Kouwenhoven, Signatures of Majorana Fermions in Hybrid Superconductor-Semiconductor Nanowire Devices, *Science* **336**, 1003 (2012).
- [8] L. P. Rokhinson, X. Liu, and J. K. Furdyna, The fractional a.c. Josephson effect in a semiconductor–superconductor nanowire as a signature of Majorana particles, *Nat. Phys.* **8**, 795 (2012).
- [9] S. Nadj-Perge, I. K. Drozdov, J. Li, H. Chen, S. Jeon, J. Seo, A. H. MacDonald, B. A. Bernevig, and A. Yazdani, Observation of Majorana fermions in ferromagnetic atomic chains on a superconductor, *Science* **346**, 602 (2014).
- [10] K. Sengupta, I. Žutić, H.-J. Kwon, V. M. Yakovenko, and S. Das Sarma, Midgap edge states and pairing symmetry of quasi-one-dimensional organic superconductors, *Phys. Rev. B* **63**, 144531 (2001).
- [11] J. Shabani, M. Kjaergaard, H. J. Suominen, Y. Kim, F. Nichele, K. Pakrouski, T. Stankevicius, R. M. Lutchyn, P. Krogstrup, R. Feidenhans'l, S. Kraemer, C. Nayak, M. Troyer, C. M. Marcus, and C. J. Palmström, Two-dimensional epitaxial superconductor-semiconductor heterostructures: A platform for topological superconducting networks, *Phys. Rev. B* **93**, 155402 (2016).
- [12] H. J. Suominen, J. Danon, M. Kjaergaard, K. Flensberg, J. Shabani, C. J. Palmström, F. Nichele, and C. M. Marcus, Anomalous Fraunhofer interference in epitaxial superconductor-semiconductor Josephson junctions, *Phys. Rev. B* **95**, 035307 (2017).
- [13] H. Ren, F. Pientka, S. Hart, A. T. Pierce, M. Kosowsky, L. Lunczer, R. Schlereth, B. Scharf, E. M. Hankiewicz, L. W. Molenkamp, B. I. Halperin, and A. Yacoby, Topological superconductivity in a phase-controlled Josephson junction, *Nature (London)* **569**, 93 (2019).
- [14] A. Fornieri, A. M. Whitticar, F. Setiawan, E. Portolés, A. C. C. Drachmann, A. Keselman, S. Gronin, C. Thomas, T. Wang, R. Kallaher, G. C. Gardner, E. Berg, M. J. Manfra, A. Stern, C. M. Marcus, and F. Nichele, Evidence of topological superconductivity in planar Josephson junctions, *Nature (London)* **569**, 89 (2019).
- [15] G. L. Fatin, A. Matos-Abiague, B. Scharf, and I. Žutić, Wireless Majorana Bound States: From Magnetic Tunability to Braiding, *Phys. Rev. Lett.* **117**, 077002 (2016).
- [16] A. Matos-Abiague, J. Shabani, A. D. Kent, G. L. Fatin, B. Scharf, and I. Žutić, Tunable magnetic textures: From Majorana bound states to braiding, *Solid State Commun.* **262**, 1 (2017).
- [17] C. T. Ke, C. M. Moehle, F. K. d. Vries, C. Thomas, S. Metti, C. R. Guinn, R. Kallaher, M. Lodari, G. Scappucci, T. Wang, R. E. Diaz, G. C. Gardner, M. J. Manfra, and S. Goswami, Ballistic superconductivity and tunable  $\pi$ -junctions in InSb quantum wells, *Nat. Commun.* **10**, 1 (2019).
- [18] S. Hart, H. Ren, M. Kosowsky, G. Ben-Shach, P. Leubner, C. Brüne, H. Buhmann, L. W. Molenkamp, B. I. Halperin, and A. Yacoby, Controlled finite momentum pairing and spatially varying order parameter in proximitized HgTe quantum wells, *Nat. Phys.* **13**, 87 (2017).
- [19] M. Hell, M. Leijnse, and K. Flensberg, Two-Dimensional Platform for Networks of Majorana Bound States, *Phys. Rev. Lett.* **118**, 107701 (2017).
- [20] F. Pientka, A. Keselman, E. Berg, A. Yacoby, A. Stern, and B. I. Halperin, Topological Superconductivity in a Planar Josephson Junction, *Phys. Rev. X* **7**, 021032 (2017).
- [21] J. Cayao, P. San-Jose, A. M. Black-Schaffer, R. Aguado, and E. Prada, Majorana splitting from critical currents in Josephson junctions, *Phys. Rev. B* **96**, 205425 (2017).
- [22] C. C. Tsuei and J. R. Kirtley, Pairing symmetry in cuprate superconductors, *Rev. Mod. Phys.* **72**, 969 (2000).

- [23] T. Yokoyama, M. Eto, and Y. V. Nazarov, Anomalous Josephson effect induced by spin-orbit interaction and Zeeman effect in semiconductor nanowires, *Phys. Rev. B* **89**, 195407 (2014).
- [24] T. Kontos, M. Aprili, J. Lesueur, F. Genêt, B. Stephanidis, and R. Boursier, Josephson Junction through a Thin Ferromagnetic Layer: Negative Coupling, *Phys. Rev. Lett.* **89**, 137007 (2002).
- [25] A. Murani, A. Kasumov, S. Sengupta, Y. A. Kasumov, V. T. Volkov, I. I. Khodos, F. Brisset, R. Delagrè, A. Chepelianskii, R. Deblock, H. Bouchiat, and S. Guéron, Ballistic edge states in Bismuth nanowires revealed by SQUID interferometry, *Nat. Commun.* **8**, 15941 (2017).
- [26] See Supplemental Material, which includes Refs. [5,11,12,14,18–20,23,27–40], at <http://link.aps.org/supplemental/10.1103/PhysRevLett.126.036802> for expanded discussion of the sample fabrication, measurements, theoretical MBS calculations, and a survey of reported measured nonmonotonic  $I_c(B)$ .
- [27] W. Mayer, M. C. Dartiailh, J. Yuan, K. S. Wickramasinghe, E. Rossi, and J. Shabani, Gate controlled anomalous phase shift in Al/InAs Josephson junctions, *Nat. Commun.* **11**, 212 (2020).
- [28] A. A. Golubov, M. Y. Kupriyanov, and G. E. Il'ichev, The current-phase relation in Josephson junctions, *Rev. Mod. Phys.* **76**, 411 (2004).
- [29] K. S. Wickramasinghe, W. Mayer, J. Yuan, T. Nguyen, L. Jiao, V. Manucharyan, and J. Shabani, Transport properties of near surface InAs two-dimensional heterostructures, *Appl. Phys. Lett.* **113**, 262104 (2018).
- [30] F. Setiawan, C.-T. Wu, and K. Levin, Full proximity treatment of topological superconductors in Josephson-junction architectures, *Phys. Rev. B* **99**, 174511 (2019).
- [31] B. Scharf, F. Pientka, H. Ren, A. Yacoby, and E. M. Hankiewicz, Tuning topological superconductivity in phase-controlled Josephson junctions with Rashba and Dresselhaus spin-orbit coupling, *Phys. Rev. B* **99**, 214503 (2019).
- [32] W. Mayer, J. Yuan, K. S. Wickramasinghe, T. Nguyen, M. C. Dartiailh, and J. Shabani, Superconducting proximity effect in epitaxial Al-InAs heterostructures, *Appl. Phys. Lett.* **114**, 103104 (2019).
- [33] C. W. Groth, M. Wimmer, A. R. Akhmerov, and X. Waintal, Kwant: A software package for quantum transport, *New J. Phys.* **16**, 063065 (2014).
- [34] J. Bardeen, R. Kümmel, A. E. Jacobs, and L. Tewordt, Structure of vortex lines in pure superconductors, *Phys. Rev.* **187**, 556 (1969).
- [35] C. W. J. Beenakker, Three “universal” mesoscopic Josephson effects, in *Transport Phenomena in Mesoscopic Systems* (Springer, New York, 1992), p. 235.
- [36] A. Haim and A. Stern, Benefits of Weak Disorder in One-Dimensional Topological Superconductors, *Phys. Rev. Lett.* **122**, 126801 (2019).
- [37] T. Laeven, B. Nijholt, M. Wimmer, and A. R. Akhmerov, Enhanced Proximity Effect in Zigzag-Shaped Majorana Josephson Junctions, *Phys. Rev. Lett.* **125**, 086802 (2020).
- [38] A. Altland and M. R. Zirnbauer, Nonstandard symmetry classes in mesoscopic normal-superconducting hybrid structures, *Phys. Rev. B* **55**, 1142 (1997).
- [39] P. San-Jose, E. Prada, and R. Aguado, ac Josephson Effect in Finite-Length Nanowire Junctions with Majorana Modes, *Phys. Rev. Lett.* **108**, 257001 (2012).
- [40] A. Altland, Y. Gefen, and G. Montambaux, What is the Thouless Energy for Ballistic Systems?, *Phys. Rev. Lett.* **76**, 1130 (1996).
- [41] M. Pakmehr, A. Khaetskii, B. D. McCombe, N. Bhandari, M. Cahay, O. Chiatti, S. F. Fischer, C. Heyn, and W. Hansen, The  $g$ -factor of quasi-two-dimensional electrons in InAs/InGaAs/InAlAs inserted-channels, *Appl. Phys. Lett.* **107**, 082107 (2015).
- [42] T. Zhou, M. C. Dartiailh, W. Mayer, J. E. Han, A. Matos-Abiague, J. Shabani, and I. Žutić, Phase Control of Majorana Bound States in a Topological X Junction, *Phys. Rev. Lett.* **124**, 137001 (2020).
- [43] M. M. Desjardins, L. C. Contamin, M. R. Delbecq, M. C. Dartiailh, L. E. Bruhat, T. Cubaynes, J. J. Viennot, F. Mallet, S. Rohart, A. Thiaville, A. Cottet, and T. Kontos, Synthetic spin-orbit interaction for Majorana devices, *Nat. Mater.* **18**, 1060 (2019).
- [44] A. Yazdani, Conjuring Majorana with synthetic magnetism, *Nat. Mater.* **18**, 1036 (2019).
- [45] J. Klinovaja and D. Loss, Time-reversal invariant parafermions in interacting Rashba nanowires, *Phys. Rev. B* **90**, 045118 (2014).